Asociación Argentina
de Mecánica Computacional

Mecánica Computacional Vol XLII, pp. 695-702
A. Caggiano, G. Etse, P. Folino, M. Goldschmit, M. Pucheta, M. Storti (Eds.)
P. Folino, M. Ripani, S. Vrech (Issue eds.)
Buenos Aires, November 11-14, 2025

ON THE PREDICTION OF DIFFUSE AND LOCALIZED FAILURE MODES FOR HIGH-PERFORMANCE CONCRETES

Sonia M. Vrech[a,b], Paula C. Folino[c,d] and Guillermo Etse[a,c]

[a]*Universidad Nacional de Tucumán, Facultad de Ciencias Exactas y Tecnología, Centro de Métodos Numéricos y Computacionales en Ingeniería, Av. Independencia 1800, Tucumán, Argentina, getse@herrera.unt.edu.ar, svrech@herrera.unt.edu.ar*

[b]*CONICET, Consejo Nacional de Investigaciones Científicas y Técnicas, Argentina*

[c]*Universidad de Buenos Aires, Facultad de Ingeniería, LMNI- Laboratorio de Métodos Numéricos en Ingeniería, Av. Las Heras 2214, Buenos Aires, Argentina, pfolino@fi.uba.ar*

[d]*Universidad de Buenos Aires-CONICET, INTECIN, Instituto de Tecnologías y Ciencias de la Ingeniería "Hilario Fernández Long", Argentina*

Keywords: Concrete, high-performance, failure, diffuse, localized.

Abstract. High-performance concretes are cementitious composites developed for particular structural or construction needs. They can include high-strength, fiber-reinforced and ultra-high-performance concretes. Those concrete types have different compositions and mechanical properties, leading to variable failure properties under given load scenarios. The focus of this work is to explore if diffuse and localized failure modes can be mathematically predicted taking as a basis the non-linear Performance Dependent Model (PDM), that has been proved to appropriately capture failure conditions for plain concretes of variable compressive strengths. The numerical results in terms of characteristic failure modes and critical directions are compared against experimental evidences.

ISSN: 2591-3522 DOI: 10.70567/mc.v42.ocsid8373

1 INTRODUCTION

A new generation of high-performance concretes which included high-strength concrete (HSC), fiber-reinforced concrete (FRC) and ultra high-performance concrete, among others, have been developed in recent years, presenting numerous advantages over the normal strength concretes (NSC) , such as higher uniaxial strengths and elasticity modulus. In order to predict their mechanic behavior, the so-called Performance Dependent Model (PDM), originally developed by Folino et al. (2009) in terms of the concrete quality, has achieved very good approximations.

In turn, according to experimental evidences, these materials generally present greater brittleness, [Naaman and Reinhardt (2006), di Prisco et al. (2009)]. Just as the transition from diffuse to localized failure modes have been numerically predicted for plain concretes, it becomes necessary to numerically analyze the influence of the reinforcements on the transition between diffuse and localized failure and on the critical surfaces directions. These aspects are addressed for the first time in this work.

After summarizing the main features of the cited constitutive model in Section 2, the mathematical indicators for diffuse and localized failure are formulated in the Section 3. Subsequently, numerical examples corresponding to uniaxial tensile and compression tests as well as direct shear ones are developed in Section 4. Finally, the main conclusions are presented in Section 5.

2 CONSTITUTIVE FORMULATION OF THE PERFORMANCE DEPENDENT MODEL

The PDM, developed by Folino et al. (2009), Folino and Etse (2011) and Folino and Etse (2012) to predict the mechanical behavior of plain concretes with variable strength through the inclusion of a performance parameter, has been extended for the case of FRC. The maximum strength criterion F_{max}, named Performance Dependent Failure Criterion (PDFC), is defined in terms of the normalized Haigh-Westergaard stress coordinates (with respect to the uniaxial compressive strength f_c'), $\overline{\xi}^*$, $\overline{\rho}^*$ and θ, as

$$\overline{\xi}^* = \frac{I_1}{\sqrt{3}}\frac{1}{f_c'} \quad , \quad \overline{\rho}^* = \sqrt{2J_2}\frac{1}{f_c'} \quad , \quad \cos(3\theta) = \frac{3\sqrt{3}}{2}\frac{J_3}{J_2^{3/2}} \quad , \tag{1}$$

being I_1 the first invariant of the stress tensor $\boldsymbol{\sigma}$, while J_2 and J_3 represent the second and third invariants of the deviatoric stress tensor $\boldsymbol{s}$. The expressions for the tension and compression meridians are given by the following parabolic equations, respectively

$$\theta = 0 \Rightarrow F_{max}^t = Ar^2\overline{\rho}_t^{*2} + B_t r\overline{\rho}_t^* + C\overline{\xi}^* - 1 = 0\,. \tag{2}$$

$$\theta = \frac{\pi}{3} \Rightarrow F_{max}^c = Ar^2\overline{\rho}_c^{*2} + B_c r\overline{\rho}_c^* + C\overline{\xi}^* - 1 = 0\,, \tag{3}$$

with the coefficients A, B_c, B_t and C, depending on f_c' and on the performance parameter β_P, computed as

$$\beta_P = \frac{1}{1000}\frac{f_c'}{(w/b)}\,, \tag{4}$$

being w/b the water-binder ratio. The ellipticity factor r is defined in terms of the eccentricity e= $\overline{\rho}_t^*/\overline{\rho}_c^*$, as

$$r = \frac{4\,(1-e^2)\cos^2\theta + (2e-1)^2}{2(1-e^2)\cos\theta + (2e-1)\sqrt{4(1-e^2)\cos^2\theta + 5e^2 - 4e}}\,. \tag{5}$$

In pre-peak or hardening regime, loading surfaces are cap-cone type: whereas the cone portion coinciding with the PDFC, remain fix, the cap portion evolves.

In post-peak or softening regime, the yield surfaces represent homogeneous contractions of the cone, according to decay softening functions based on fracture energy concepts.

The formulation is complemented by an associated plastic flow in hardening regime. Whereas in softening, a volumetric non-associated flow, that only differ from the yield surface in the volumetric component, is defined. For a complete description of the model, please refer to Folino and Etse (2012).

3 FAILURE INDICATORS

In the framework of the Smeared Crack Approach, three different forms of failure can be distinguished as the load increases: diffuse, localized and discrete. From a mathematical point of view, the jumps in the rate of the kinematic fields, i.e. displacements $[[\dot{\boldsymbol{u}}]]$ and deformations $[[\dot{\boldsymbol{\varepsilon}}]]$, characterize the failure modes according to Table 1.

Failure	Displacement field	Strain field
Diffuse	Continuous (C^1) - $[[\dot{\boldsymbol{u}}]] = 0$	$[[\dot{\boldsymbol{\varepsilon}}]] = 0$
Localized	Continuous (C^0) - $[[\dot{\boldsymbol{u}}]] = 0$	$[[\dot{\boldsymbol{\varepsilon}}]] \geq 0$
Discrete	Discontinuous - $[[\dot{\boldsymbol{u}}]] \geq 0$	$[[\dot{\boldsymbol{\varepsilon}}]] \geq 0$

Table 1: Kinematic conditions of failure modes.

3.1 Diffuse failure indicators

The mathematical indicator of diffuse failure is adopted as the classical Hill instability criterion by Hill (1958), given by the energetic delimiter, i.e. the second-order work density $d^2W = 0$, leading to the stationary stress condition $\dot{\boldsymbol{\sigma}} = \mathbf{0}$, being $\dot{\boldsymbol{\sigma}}$ the stress tensor rate. This condition implies the singularity of the elasto-plastic tangent material tensor, as

$$det\left(\boldsymbol{E}^{EP}\right) = 0\,. \tag{6}$$

Non-associative flow rules give rise to non-symmetric elasto-plastic tangent operators. The vanishing determinant of the symmetric part of the tangent operator, provides a more critical lower bound condition according to the Bromwich bounds, as

$$det\left(\boldsymbol{E}^{EP}_{sym}\right) = 0\,. \tag{7}$$

Consequently, in this case, the loss of stability takes place before the limit point condition ($\dot{\boldsymbol{\sigma}} = \mathbf{0}$) is reached. In this case, the critical hardening modulus may stills be positive.

3.2 Localized failure indicator

The localization condition, based on the early works of Hadamard (1903); Thomas (1961); Hill (1958, 1962), characterized through a discontinuity in the rate of the displacement gradient while the displacement rate remains continuous, is given by the singularity of the elasto-plastic acoustic tensor, as

$$det\left(\boldsymbol{Q}^{EP}\right) = 0 \quad \text{with} \quad \boldsymbol{Q}^{EP} = \boldsymbol{N} \cdot \boldsymbol{E}^{EP} \cdot \boldsymbol{N}\,, \tag{8}$$

being $\boldsymbol{N}$ the unit vector normal to the discontinuity surface, see Fig. 1. By varying $\boldsymbol{N}$ between 0 and 180°, Eq. (8) is computed and the localized failure direction α is obtained when the condition $det(Q)^{EP} \leq 0$ is satisfied.

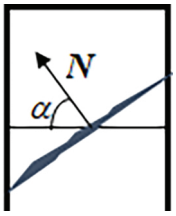

Figure 1: Diagram of the localized failure.

4 NUMERICAL APPLICATIONS

In this section, failure modes and critical directions for FRC are numerically predicted regarding simple load states at material level. Uniaxial tensile and compression as well as direct shear tests are evaluated.

To this end, the material properties corresponding to the samples used in the experimental campaigns by Folino et al. (2020) and Xargay et al. (2018) are taken into account, i.e.

- Plain concretes with f'_c= 30 and 80 MPa (NSC and HSC, respectively).
- FRC with a steel fibers content of 0.50% in volume fraction (40 kg/m^3).
- FRC with a steel fibers content of 0.75% in volume fraction (60 kg/m^3).

The benefits of the reinforcement on the overall mechanical behavior can be appreciated in Fig. 2, where the curves of recorded loads in terms of the crack mouth opening displacements (CMOD) evolution for the three point bending tests (TPB) are depicted. Increased stiffness, strength and fracture energy, especially in the case of NSC, can be observed.

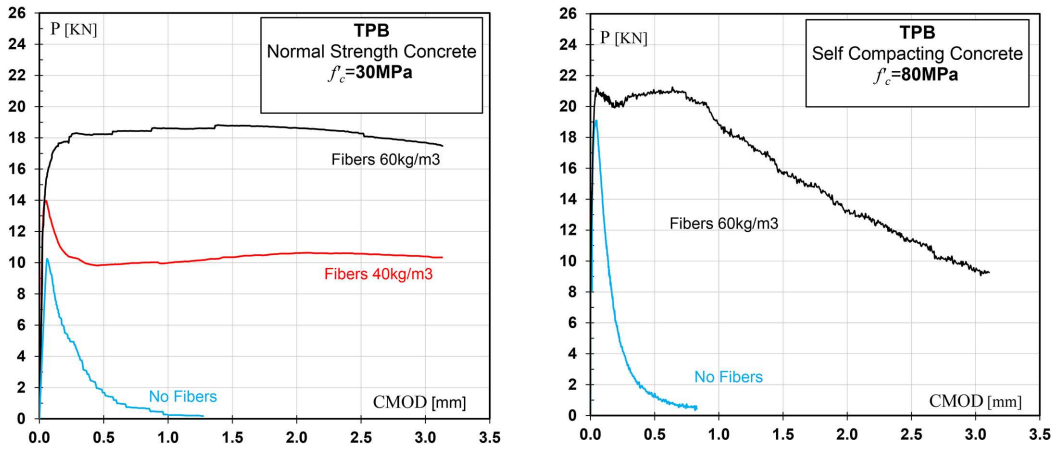

Figure 2: TPB tests. (a) NSC by Folino et al. (2020); (b) HSC by Xargay et al. (2018).

4.1 Uniaxial tensile test

First, the uniaxial tensile test is considered and the normalized localized failure indicator $det(\boldsymbol{Q})^{EP}/det(\boldsymbol{Q})^{E}$ is analyzed at the peak. Fig. 3 shows brittle failure modes preceding the peak for both, plain NSC (a) and HSC (b). The addition of steel fibers delays it until the peak but maintaining the same critical angles.

Localization directions are α= 70° and 110° for NSC, while for HSC result α= 73° and 107°. Moreover, more negative indicator values are obtained for HSC, indicating greater fragility. These results are in agreement with the experimental evidences, shown in Fig. 4.

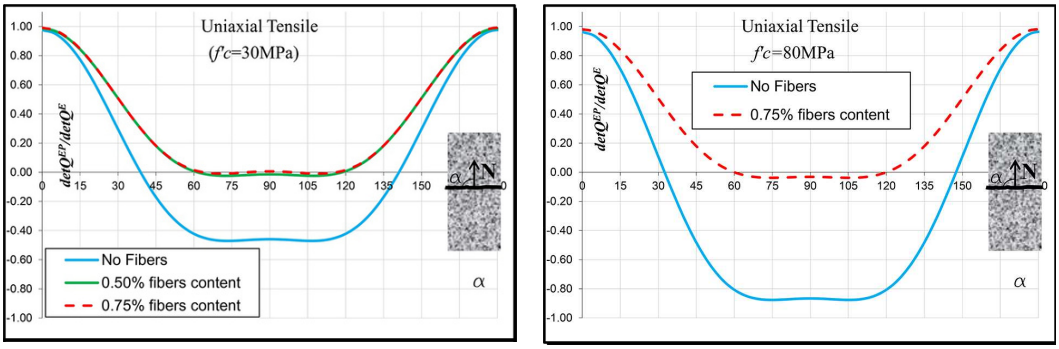

(a) (b)

Figure 3: Numerical localization analysis of the uniaxial tensile test. (a) NSC; (b) HSC.

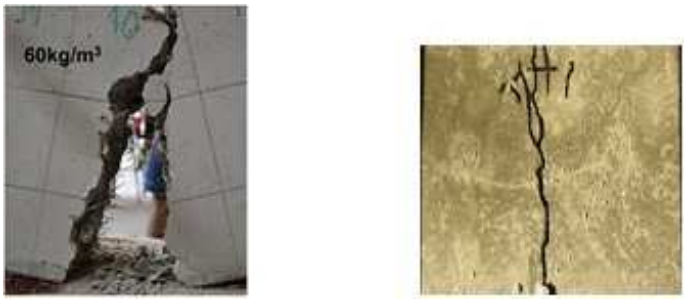

(a) (b)

Figure 4: Final view of FRC specimens after the TPB. (a) NSC; (b) HSC.

4.2 Uniaxial compression test

As is well known, steel fibers addition not necessary leads to an increase of the compressive strength. Likewise, no notable differences are observed regarding failure properties for plain and reinforced concretes.

Diffuse failure modes has been obtained for all cases. For plain NCS, α= 23°. With the addition of fibers, the cracks tend to be parallel to the load direction being α= 21°, see Fig. 5-(a).

In case of HSC, this effect is negligible. According Fig. 5-(b), the critical angle results more parallel to the loading direction than for NSC, being α= 20°. This is shown in Fig. 6-(a), corresponding to the end of the uniaxial compression test by Xargay et al. (2018).

4.3 Direct shear test

For all cases, the direct shear test leads to brittle failure surfaces located to 25° and 65°, as can be appreciated in the polar plots of Fig. 7, in agreement the 63° observed by Soltanzadeh et al. (2015) for HSC with f'_c= 68MPa, see Fig. 6-(b).

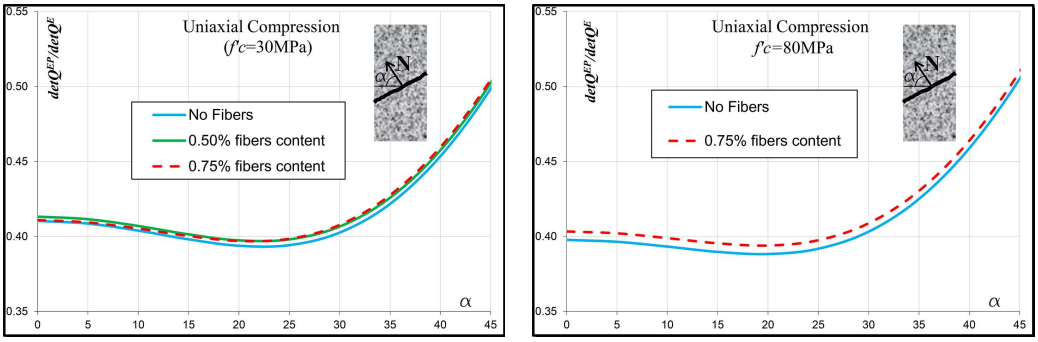

(a) (b)

Figure 5: Numerical localization analysis of the uniaxial compression test. (a) NSC; (b) HSC

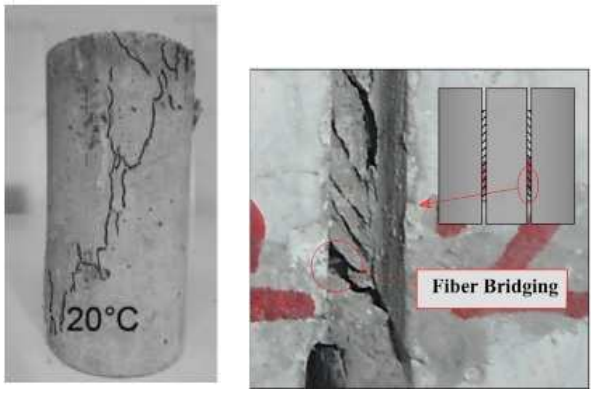

(a) (b)

Figure 6: Failure patterns of fiber-reinforced HSC. (a) Uniaxial compression test by Xargay et al. (2018); (b) Direct shear test by Soltanzadeh et al. (2015).

The effect of fibers in delaying localized failure is notable for both, NSC in Fig. 7-(a) and HSC in (b). The latter, when unreinforced, demonstrate greater fragility with higher failure indicator values than NSC.

5 CONCLUSIONS

This work presents the application of an elasto-plastic numerical approach, the Performance Dependent Model, extended to simulating the failure behavior of high-performance concretes at material level, particularly FRC.

Failure modes and critical directions have been numerically evaluated for simple loading states, obtaining good approximations with the experimental evidences. Uniaxial tension and compression test as well as the direct shear one have been considered.

Under uniaxial tension and shear conditions, plain concrete exhibits localized failure even in the pre-peak regime. The addition of steel fibers delays this process. For uniaxial compression conditions, no significant fiber contributions are evident. The obtained critical angles are consistent with experimental evidence in all cases.

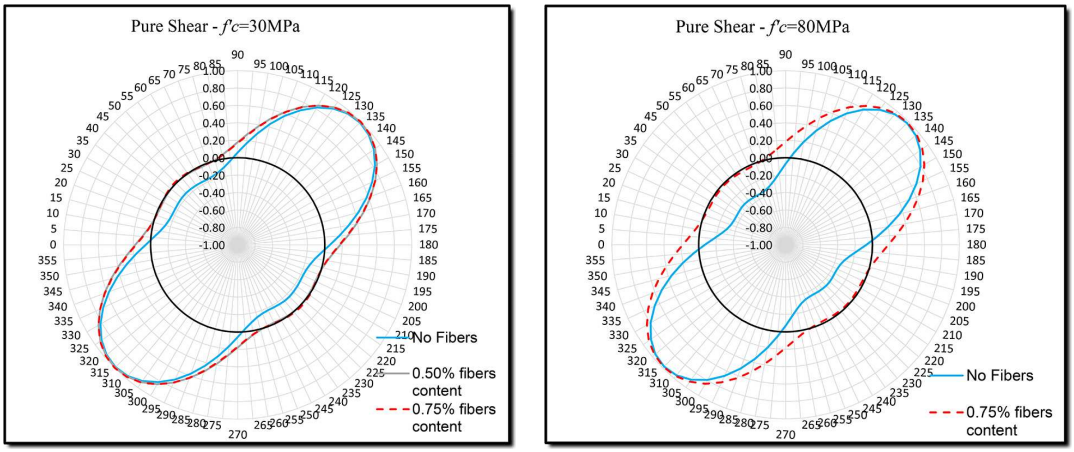

(a) (b)

Figure 7: Numerical localization analysis of the direct shear test. (a) NSC; (b) HSC

ACKNOWLEDGEMENTS

The authors acknowledges to CONICET (National Scientific and Technical Research Council), University of Buenos Aires and National University of Tucuman, Argentina, for the funding provided through the Grants no. 23120180100014CO, UBACYT 20020220100185B and PIUNT E754, respectively.

REFERENCES

di Prisco M., Plizzari G., and Vandewalle L. Fibre reinforced concrete: new design perspectives. *Mater Struct.*, 42:1261–1281, 2009. http://doi.org/10.1617/s11527-009-9529-4.

Folino P. and Etse G. Validation of the performance dependent failure criterion for concretes. *ACI Materials Journal*, 108(3):261–269, 2011. http://doi.org/10.14359/51682491.

Folino P. and Etse G. Performance dependent model for normal and high strength concretes. *International Journal of Solids and Structures*, 49(5):701–719, 2012. http://doi.org/10.1016/j.ijsolstr.2011.11.020.

Folino P., Etse G., and Will A. A performance dependent failure criterion for normal and high strength concretes. *ASCE Journal of Engineering Mechanics*, 135(12):1393–1409, 2009.

Folino P., Ripani M., Xargay H., and Rocca N. Comprehensive analysis of fiber reinforced concrete beams with conventional reinforcement. *Engineering Structures*, 202:109862, 2020. http://doi.org/10.1016/j.engstruct.2019.109862.

Hadamard J. *Lecons sur la Propagation des Ondes*. Librairie Scientifique A. Hermann et Fils, Paris, 1903.

Hill R. A general theory of uniqueness and stability in elastic-plastic solids. *J. Mech. Phys. Solids*, 6:239–249, 1958.

Hill R. Acceleration waves in solids. *J. Mech. Phys. Solids*, 10:1–16, 1962.

Naaman A. and Reinhardt H. Proposed classification of HPFRC composites based on their tensile response. *Mater Struct.*, 39:547–555, 2006. http://doi.org/10.1617/s11527-006-9103-2.

Soltanzadeh F., Barros J., and Santos R. High performance fiber reinforced concrete for the shear reinforcement: experimental and numerical research. *Construct Build Mater.*, 77:94–109, 2015. http://doi.org/10.1016/j.conbuildmat.2014.12.003.

Thomas T. *Plastic Flow and Fracture of Solids*. Academic Press, New York, 1961.

Xargay H., Folino P., Sambataro L., and Etse G. Temperature effects on failure behavior of self-compacting high strength plain and fiber reinforced concrete. *Construction and Building Materials*, 165:723–734, 2018. http://doi.org/10.1016/j.conbuildmat.2017.12.137.